RESEARCH ARTICLE SUMMARY

ALZHEIMER'S DISEASE

Amyloid β oligomers constrict human capillaries in Alzheimer's disease via signaling to pericytes

Ross Nortley, Nils Korte*, Pablo Izquierdo*, Chanawee Hirunpattarasilp*, Anusha Mishra*, Zane Jaunmuktane*, Vasiliki Kyrargyri*, Thomas Pfeiffer, Lila Khennouf, Christian Madry, Hui Gong, Angela Richard-Loendt, Wenhui Huang, Takashi Saito, Takaomi C. Saido, Sebastian Brandner, Huma Sethi, David Attwell†

INTRODUCTION: In Alzheimer's disease (AD), the production of amyloid β (Aβ) oligomers and downstream tau dysfunction are thought to cause neuronal damage, in particular a loss of synapses and synaptic plasticity, which results in cognitive impairment. However, epidemiological data show that vascular factors are important contributors to AD risk, and biomarker research has shown that the first change in AD is a decrease of cerebral blood flow. Because most of the vascular resistance within the brain is located in capillaries, this could reflect a dysfunction of contractile pericytes on capillary walls. Indeed, pericytes are known to regulate cerebral blood flow physiologically and to severely restrict blood flow after stroke.

RATIONALE: We examined the role of pericytes in Alzheimer's disease by examining cerebral capillaries in humans and mice developing AD, and by applying Aβ to capillaries. We used freshly fixed brain biopsies from cognitively impaired living humans who were depositing Aβ plaques, and also carried out in vivo imaging in a knock-in mouse model of AD. We measured capillary diameters at positions near pericytes in order to assess whether the capillaries became constricted in AD, because this would lead to a decrease of cerebral blood flow and hence a decrease of the glucose and oxygen supply to the brain tissue. In addition, to investigate one mediator already thought to be important in AD, we applied Aβ to human brain slices made from normal tissue that was removed from patients undergoing neurosurgical glioma resection, as well as to rodent brain slices. Aβ was applied in the oligomeric form, which is thought to contribute to cognitive decline. This allowed us to examine whether Aβ itself might alter cerebral blood flow, and to use pharmacology to investigate the mechanism of any such effect.

RESULTS: Both in humans developing AD and in the mouse model of AD, capillaries were constricted specifically at pericyte locations, but arterioles and venules were unchanged in diameter. Thus, the reduction of cerebral blood flow known to occur in AD is produced by capillaries rather than by arterioles. The capillary constriction increased rapidly with the severity of Aβ deposition, and we calculated that in the human cortex this constriction would have the effect of reducing cerebral blood flow by approximately half; this is comparable to the decrease of blood flow measured experimentally in affected parts of the AD brain. In the AD mouse cerebellum, which lacks Aβ deposition at the age examined, there was no capillary constriction, supporting the idea of a causal link between Aβ level and constriction of capillaries. Aβ itself was found to constrict both human and rodent capillaries through a mechanism involving the generation of reactive oxygen species (ROS), mainly by NOX4 (reduced nicotinamide adenine dinucleotide phosphate oxidase 4). The ROS then triggered the release of endothelin-1, which acted on ET_A receptors to evoke pericyte contraction, thus causing capillary constriction. The Aβ-evoked constriction could be halted by blocking NOX4 and ET_A receptors, and was reversed by applying the vasodilator C-type natriuretic peptide.

CONCLUSION: These data reconcile genetic evidence for a role of Aβ in triggering neuronal damage and cognitive decline in AD with the fact that a decrease of cerebral blood flow is the first clinically detectable change in AD. They imply that attention should be given to vascular mechanisms in AD as well as to signaling pathways that act directly on neurons or glia, and suggest novel therapeutic approaches for treating early AD by targeting drugs to brain pericytes. Our findings also raise the question of what fraction of the damage to synapses and neurons in AD reflects direct actions of Aβ and downstream tau, and what fraction is a consequence of the decrease of energy supply that Aβ produces by constricting capillaries. ■

ON OUR WEBSITE

Read the full article at http://dx.doi.org/10.1126/science.aav9518
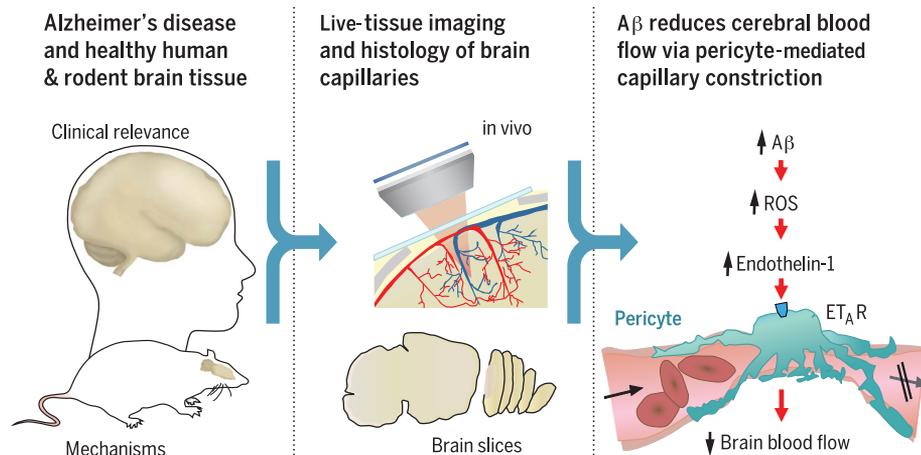
Live human and rodent brain capillaries become constricted in Alzheimer's disease.
Tissue from humans and rodents (left) that were healthy or developing Alzheimer's disease (AD) was imaged in vivo and as brain slices (center), revealing that pericytes constrict brain capillaries early in AD via a mechanism involving ROS generation and release of endothelin-1, which activates ET_A receptors (right).

RESEARCH ARTICLE

Amyloid β oligomers constrict human capillaries in Alzheimer's disease via signaling to pericytes

Ross Nortley[1], Nils Korte[1]*, Pablo Izquierdo[1]*, Chanawee Hirunpattarasilp[1]*,
Anusha Mishra[2]*, Zane Jaunmuktane[3,4]*, Vasiliki Kyrargyri[1]*†, Thomas Pfeiffer[1],
Lila Khennouf[1], Christian Madry[1]‡, Hui Gong[1], Angela Richard-Loendt[3],
Wenhui Huang[5], Takashi Saito[6], Takaomi C. Saido[6], Sebastian Brandner[3,7],
Huma Sethi[8], David Attwell[1]§

Cerebral blood flow is reduced early in the onset of Alzheimer's disease (AD). Because most of the vascular resistance within the brain is in capillaries, this could reflect dysfunction of contractile pericytes on capillary walls. We used live and rapidly fixed biopsied human tissue to establish disease relevance, and rodent experiments to define mechanism. We found that in humans with cognitive decline, amyloid β (Aβ) constricts brain capillaries at pericyte locations. This was caused by Aβ generating reactive oxygen species, which evoked the release of endothelin-1 (ET) that activated pericyte ET_A receptors. Capillary, but not arteriole, constriction also occurred in vivo in a mouse model of AD. Thus, inhibiting the capillary constriction caused by Aβ could potentially reduce energy lack and neurodegeneration in AD.

Vascular compromise occurs early in Alzheimer's disease (AD) (*1*, *2*). Cerebral blood flow in the gray matter can be reduced by more than 40% (*3*); indeed, reduced cerebral blood flow is the earliest biomarker of the development of the disease (*1*). Around the time that the amyloid hypothesis for AD was proposed (*4*–*6*), it was reported that capillaries in the brains of AD patients showed an abnormal, focally constricted morphology (*7*). Although much succeeding work focused on amyloid β (Aβ)– and tau-evoked damage to neurons, increasing evidence suggests a role for vascular disturbance in the onset of AD (*8*, *9*). Exogenous Aβ can reduce cerebral blood flow (*10*–*12*), and reduced blood flow increases Aβ production (*13*, *14*).

Investigations of the vascular effects of exogenous Aβ have focused on arteries and arterioles (*12*, *15*), but the majority of the vascular resistance within the brain is located in capillaries (*16*). Capillary dysfunction correlates with cognitive decline in AD (*17*). This suggests that capillaries could be the most important locus where Aβ produced within the brain can act to decrease cerebral blood flow. A subset of pericytes on capillary walls is contractile [these are the only contractile cells on capillaries (*18*)] and can alter cerebral blood flow by adjusting their contractile tone (*18*–*20*). In a rodent model of AD, there are disturbances of unknown origin in the control of capillary blood flow (*21*). We therefore investigated how pericytes were affected by exogenous and endogenously generated Aβ, and in particular by Aβ$_{1–42}$ oligomers, the molecular species believed to be responsible for Aβ's toxic effects in AD (*22*, *23*). To maximize the relevance to human disease, we used living human brain slices derived from neurosurgically resected brain tissue to study acute responses to Aβ, and rapidly fixed human brain biopsy tissue (from living patients with or without Aβ deposition) to assess pericyte responses to long-term accumulation of endogenous Aβ in AD. The effects seen in human tissue were also seen in vivo in a transgenic mouse model of AD and were analyzed mechanistically in brain slices.

Amyloid β constricts human capillaries at pericytes

Living human brain cortex slices were obtained from tissue removed during neurosurgical operations to access tumors (see materials and methods)

and either fixed for immunohistochemistry or imaged live to study pericyte properties. Labeling the basement membrane with fluorescently tagged isolectin B$_4$ (IB$_4$), or immunolabeling for the pericyte marker PDGFRβ (platelet-derived growth factor receptor β), revealed pericyte morphology. Pericytes were observed with a classical "bump-on-a-log" morphology on the straight parts of capillaries, or at their branch points, with processes extending along and around the capillaries (Fig. 1, A and B). With experience, morphology alone was sufficient to identify pericytes reliably in brain slices (fig. S1). The mean distance between human pericytes was 65.3 ± 0.4 µm (for 94 pericytes imaged in tissue from two patients), 30% larger than in rodents (*19*). As for arteriole smooth muscle cells (Fig. 1C), the processes of 36% of pericytes could be labeled for α smooth-muscle actin (Fig. 1D) [the real percentage may be higher with different fixation techniques (*24*)], providing a mechanistic basis for the Aβ-evoked contraction (see below). In human brain slices, as previously reported for rodent capillaries (*18*, *19*), superfused noradrenaline constricted and glutamate dilated the capillaries at pericyte locations (Fig. 1, E and F). This is consistent with the circumferential processes of pericytes (which are oriented to be able to reduce capillary diameter) being preferentially found near pericyte somata (fig. S2), so that capillary constriction by pericytes occurs predominantly near these somata (fig. S3). Thus, the surgery-derived human tissue had functioning contractile pericytes (Fig. 1, E and F).

Aβ was oligomerized (see materials and methods), and silver staining of SDS–polyacrylamide gel electrophoresis (PAGE) gels was used to assess the degree of aggregation of the Aβ isoforms. The predominant species produced (other than monomers) for Aβ$_{1–42}$ and Aβ$_{1–40}$ had a molecular weight 2 to 4 times that of monomers, whereas scrambled Aβ$_{1–42}$ formed mainly monomers (Fig. 1G). Applying soluble Aβ$_{1–42}$ (oligomeric + monomeric, 72 nM calculated from the monomeric molecular weight) to human brain slices evoked a slowly developing constriction of all four capillaries tested, which reduced their diameter by ~25% after 40 min (Fig. 1H, significantly reduced, $P = 0.01$).

Because the limited availability of live human tissue precluded detailed analysis of the mechanism underlying the Aβ-evoked constriction, we carried out experiments on rat cortical slices. As for human capillaries, Aβ$_{1–42}$ evoked a constriction of rat capillaries near pericyte locations that was visible using either bright-field illumination or two-photon fluorescence imaging of IB$_4$ (Fig. 2, A, B, C, and G). Of 20 capillaries tested, 16 (80%) showed a >5% constriction in response to Aβ$_{1–42}$. The time course of the mean Aβ$_{1–42}$-evoked constriction (including all vessels) was similar (Fig. 2C) to that in human cortex (Fig. 1H), reaching ~15% after 1 hour ($P = 0.006$). Aβ$_{1–40}$ also evoked a similar constriction (Fig. 2, C and G; $P = 0.048$) in five of six capillaries tested (83%). Capillaries monitored for an hour without applying Aβ, or those to which a version of Aβ$_{1–42}$

Fig. 1. Oligomeric Aβ acts on pericytes to constrict capillaries in human brain slices. (**A**) IB$_4$-labeled capillary in a human cortical slice, with two pericyte somata (white arrowheads) outlined by their basement membrane. Nuclei are stained with DAPI (blue). (**B**) Pericyte labeled with antibody to PDGFRβ. (**C** and **D**) Arteriole (C) and pericyte (D) labeled with IB$_4$ and antibody to α smooth muscle actin (α-SMA, localized in processes originating from the pericyte soma). (**E**) Images of a capillary (red lines between yellow arrowheads indicate diameter) and pericyte soma (white arrowheads) in a live human brain slice before drug application, in the presence of 2 μM superfused noradrenaline (+NA), with 2 μM NA and 500 μM glutamate superfused (+NA +Glu), and after stopping drug superfusion (washout). Graph shows time course of capillary diameter at red line throughout the experiment. (**F**) Mean (± SEM) glutamate-evoked dilation and noradrenaline-evoked constriction in experiments as in (E) (numbers of pericytes on bars; change in diameter was quantified relative to that before application of each drug; relative to the pre-noradrenaline diameter, the glutamate-evoked dilation was 26.8 ± 7.7%). (**G**) Silver staining of an SDS-PAGE gel for Aβ solutions prepared as in materials and methods. (**H**) Images of a human capillary before and after superfusion of 72 nM Aβ$_{1-42}$, showing a region (red line) being constricted by a pericyte (arrowheads). Graph shows mean (±SEM) diameter change at four pericyte locations from four slices treated with Aβ and three pericyte locations from three slices superfused with aCSF lacking Aβ (significantly reduced at 40 min in Aβ, $P = 0.01$).

with a scrambled sequence was applied (prepared as for the Aβ oligomers), showed no significant diameter change (Fig. 2, C and G). Scrambled Aβ$_{1-42}$ mainly formed monomers (Fig. 1G; see also materials and methods), unlike Aβ$_{1-42}$ and Aβ$_{1-40}$, which may indicate that oligomer formation is obligatory for an effect on pericytes. The pericyte-mediated constriction evoked by Aβ$_{1-42}$ showed a Michaelis-Menten dependence on Aβ concentration, with an apparent EC$_{50}$ (the concentration for a half-maximal response, equal to the Michaelis constant K_m obtained by fitting a Michaelis-Menten relation to the data) of 4.7 nM (Fig. 2D).

Reactive oxygen species and endothelin-1 generate the capillary constriction

We blocked Aβ$_{1-42}$-evoked capillary constriction in rat cortical slices by means of the endothelin-1 (ET) type A receptor blocker BQ-123 (1 μM, $P = 0.008$; Fig. 2, E and G); by application of superoxide dismutase 1 (SOD1, 150 units/ml; $P = 3.7 \times 10^{-6}$; Fig. 2, E and G), which scavenges reactive superoxide generated when Aβ activates reduced nicotinamide adenine dinucleotide phosphate (NADPH) oxidase (and prevents hydroxyl radical formation by the Fenton reaction); or by inhibiting NADPH oxidase with diphenyleneiodonium (DPI, 10 μM, $P = 0.032$; Fig. 2, F and G). In contrast, applying these agents alone did not affect capillary diameter (changes after 1 hour: BQ-123, −0.7 ± 5.2%, $n = 13$, $P = 0.9$; SOD1, 3.4 ± 5.8%, $n = 9$, $P = 0.57$; DPI, −7.4 ± 3.2%, $n = 5$, $P = 0.082$). The Aβ$_{1-40}$-evoked capillary constriction was also abolished by BQ-123 (a 6.2 ± 1.6% dilation was seen after 1 hour of Aβ$_{1-40}$ applied in BQ-123, $n = 5$), contradicting the suggestion (25) that

Aβ$_{1-40}$ does not evoke ET release. These results suggest the involvement of NADPH oxidase–mediated reactive oxygen species (ROS) generation and ET release in the Aβ-evoked capillary constriction. Reactive nitrogen species derived from superoxide were not involved, because inhibiting nitric oxide synthase (NOS) with 100 μM N$_\omega$-nitro-L-arginine (L-NNA) had no effect ($P = 0.83$) on the Aβ-evoked constriction (Fig. 2, F and G); L-NNA alone had no effect (after 1 hour, the diameter change was −0.5 ± 7.9%, $n = 6$, $P = 0.99$). The fact that Aβ evoked constrictions even in the presence of L-NNA also rules out the possibility that Aβ-evoked ROS production caused constriction (26) by ROS binding to, and removing, vasodilatory NO. The NOX4 (NADPH oxidase 4) blocker GKT137831 (0.45 μM) abolished the Aβ-evoked capillary constriction (Fig. 2, F and G;
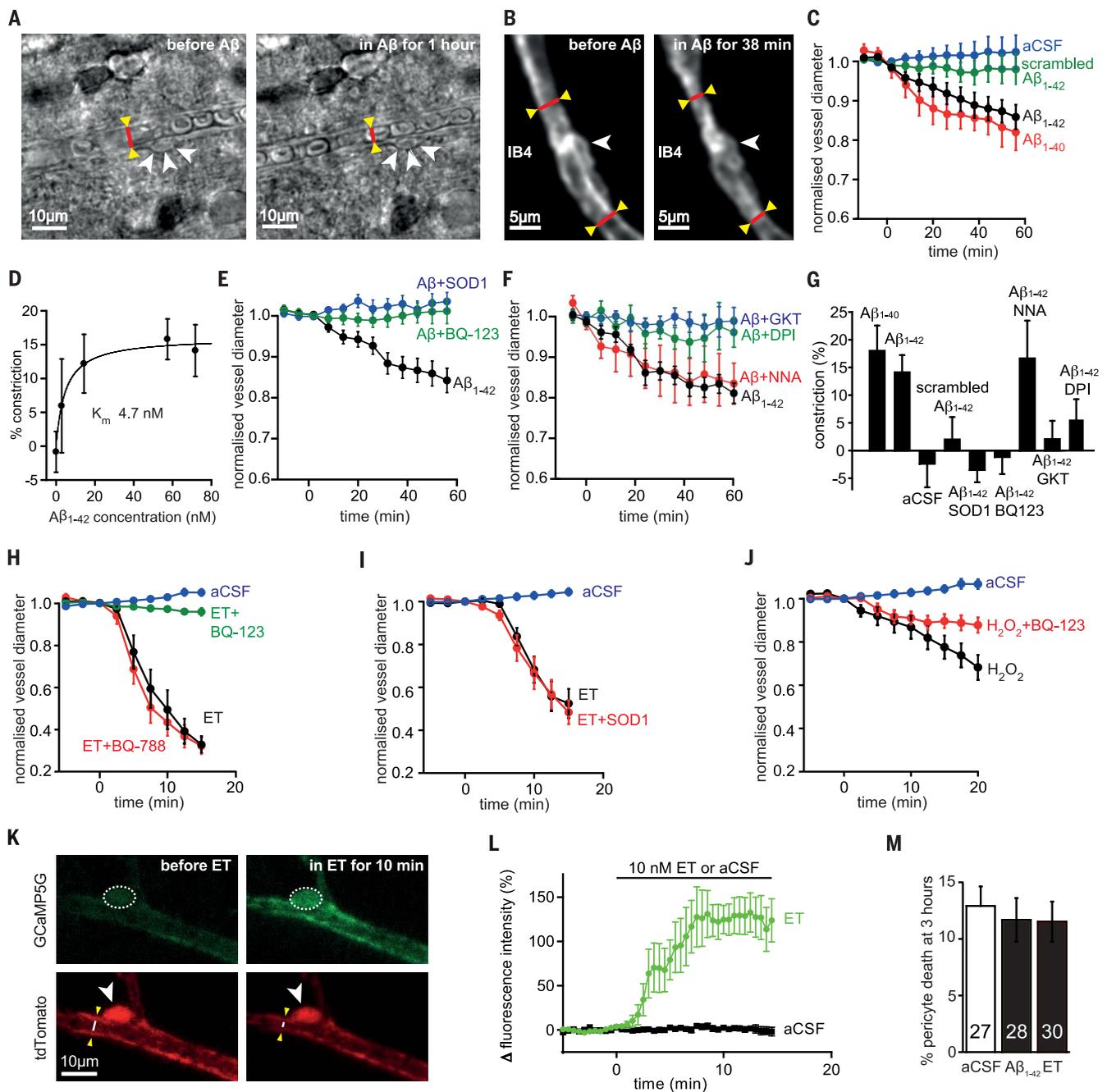
Fig. 2. Aβ acts via ROS and ET_A receptors. (**A** and **B**) Bright-field images (A) and two-photon–evoked IB4 fluorescence (B) of capillaries in rat cortical slices in aCSF and after applying 72 nM Aβ_{1–42}, showing constriction (yellow arrowheads and red lines) near pericytes (white arrowheads, compare with figs. S2 and S3). (**C**) Mean (± SEM) time course of capillary diameter during superfusion with aCSF (n = 51 vessels), 109 nM scrambled Aβ_{1–42} (n = 32), 72 nM Aβ_{1–42} (n = 20), or 100 nM Aβ_{1–40} (n = 6). (**D**) Constriction evoked after 1 hour by different concentrations of Aβ_{1–42} (0 nM, n = 51; 2.9 nM, n = 11; 14 nM, n = 10; 57 nM, n = 19; 72 nM, n = 20). Curve is a Michaelis-Menten relation with a K_m of 4.7 nM and a maximum of 16.1%. (**E** to **J**) Time course of diameter when applying the following agents (experiments in each panel were interleaved; blockers were present for 5 to 15 min before Aβ). (E) 57 nM Aβ_{1–42} alone (n = 19) or in the presence of SOD1 (150 units/ml, n = 19) or the ET_A blocker BQ-123 (1 µM, n = 14). (F) 72 nM Aβ_{1–42} alone (n = 7) or in the presence of the NOS blocker L-NNA (100 µM, n = 6), the NADPH oxidase blocker DPI (10 µM, n = 5), or the

NOX4 blocker GKT137831 (0.45 µM, n = 7). (G) Constriction produced at 60 min for (C) to (F). (H) Effect of aCSF (n = 10), ET alone (10 nM, n = 10), or ET in the presence of the ET_A blocker BQ-123 (1 µM, n = 10) or the ET_B blocker BQ-788 (1 µM, n = 12). (I) aCSF or ET (5 nM) in the absence (n = 12) or presence of SOD1 (150 units/ml, n = 8). (J) aCSF or the ROS generator H_2O_2 (1 mM, n = 9, which evokes constriction: $P = 1.1 \times 10^{-5}$ at 20 min) or H_2O_2 with the ET_A blocker BQ-123 (1 µM, n = 11, constriction is reduced, P = 0.009). (**K**) Two-photon image of mouse cortical pericyte expressing GCaMP5G (green), before and while applying ET (10 nM), which raises [Ca^{2+}]_i (increase in green intensity) in pericyte soma (arrowhead; dashed line shows ROI analyzed) and processes, and constricts the capillary (see white line on image of the tdTomato reporter of GCaMP5G expression, red). (**L**) Mean [Ca^{2+}]_i time course in eight pericyte somata in response to ET (significantly elevated, P = 0.0014) and in seven somata in aCSF (no significant change, P = 0.74). (**M**) Incubating rat brain slices (numbers on bars) with Aβ_{1–42} oligomers (1.4 µM) or ET (100 nM) for 3 hours does not increase pericyte death.
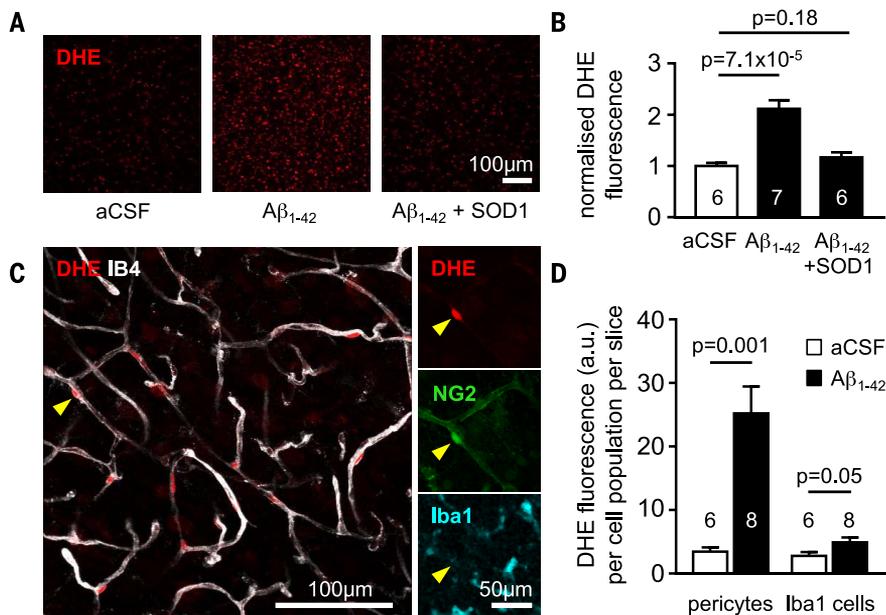
Fig. 3. Aβ evokes ROS generation in pericytes. (**A**) Fluorescence images of dihydroethidium (DHE)–loaded rat cortical slices incubated in control aCSF or aCSF containing Aβ$_{1-42}$ (72 nM) or Aβ$_{1-42}$ + SOD1 (150 units/ml) for 40 min, showing that Aβ increases ROS level and that this is inhibited by SOD1. (**B**) Fluorescence (normalized to value in aCSF, mean ± SEM) of slices incubated in aCSF ($n = 6$), Aβ$_{1-42}$ ($n = 7$), or Aβ$_{1-42}$ + SOD1 ($n = 6$). (**C**) Left: Image of a cortical slice showing that the brightest DHE-labeled cells are located on IB$_4$-labeled blood vessels (arrowhead). Right: Immunolabeling shows that these cells colocalize with NG2 but not with Iba1, implying that they are pericytes rather than microglia or perivascular macrophages. (**D**) Soma DHE fluorescence [arbitrary units (a.u.), mean ± SEM] from the population of pericytes, or of Iba1-labeled cells, after 40 min in the absence or presence of Aβ$_{1-42}$. Numbers on bars are slices (fluorescence was averaged across three image stacks for each slice).

$P = 0.0011$) but did not affect diameter when applied alone (changed by $5.7 \pm 5.6\%$, $n = 6$, $P = 0.35$ after 1 hour), whereas the NOX2 blocker ebselen (2 μM) reduced the constriction by only 45% ($n = 8$, $P = 0.027$); on its own, ebselen had no effect (diameter changed by $1.4\% \pm 3.8\%$, $n = 9$, $P = 0.8$ after 1 hour). These data suggest that NOX4 in pericytes or endothelial cells (27–29), rather than NOX2 in immune cells (28, 29), is the NADPH oxidase mainly responsible for generating the ROS that evoke capillary constriction. Data presented in Fig. 3 suggest that the NOX4 producing the ROS is in pericytes.

To confirm that pericytes constrict in response to activation of ET receptors, we applied ET (10 nM) either alone or with a blocker of its type A (ET$_A$) or type B (ET$_B$) receptors. Endothelin-1 evoked a strong (>65%) pericyte-mediated constriction of capillaries ($P = 2 \times 10^{-12}$), which was blocked by the ET$_A$ blocker BQ-123 (1 μM, $P = 2.6 \times 10^{-11}$) but not by the ET$_B$ blocker BQ-788 (1 μM, $P = 0.91$; Fig. 2H). ET still evoked a constriction in the presence of SOD1 ($P = 1.3 \times 10^{-8}$; Fig. 2I), implying that ET acts downstream of ROS. Use of H$_2$O$_2$ (1 mM) to generate ROS evoked a constriction ($P = 1.1 \times 10^{-5}$) that was reduced by BQ-123 ($P = 0.009$; Fig. 2J), which suggests that ROS evoke constriction via ET$_A$ receptor activation. Consistent with the idea that ET$_A$ receptors that generate pericyte contraction

are on the pericytes themselves, we found that in pericytes expressing GCaMP5G (see materials and methods), applying ET (10 nM) evoked a rise in intracellular calcium concentration [Ca^{2+}]$_i$, whereas artificial cerebrospinal fluid (aCSF) had no effect (Fig. 2, K and L). These data establish Aβ$_{1-42}$-evoked generation of ROS as being upstream of the elevated level (30, 31) [or potentiated effect (32)] of ET that makes pericytes constrict capillaries.

In profound ischemia, pericyte-evoked constriction of capillaries is followed by the pericytes dying necrotically in rigor (caused by an excessive rise of [Ca^{2+}]$_i$), thus maintaining a decreased capillary diameter and a long-lasting decrease of blood flow (19). Pericytes also die after accumulating Aβ in AD (33). We assessed whether exposure to 1.4 μM soluble Aβ$_{1-42}$ or 100 nM ET for 3 hours had a similar effect on pericyte health by applying propidium iodide to label cells with membranes that had become nonspecifically permeable, as occurs in ischemia (19). These treatments did not significantly increase pericyte death on this time scale (Fig. 2M; $P = 0.85$ for Aβ$_{1-42}$, $P = 0.59$ for ET).

To assess which cell types generated ROS in response to Aβ, in brain slices we used imaging of the ROS sensor dihydroethidium, which generates fluorescence when oxidized dihydroethidium intercalates into DNA (see materials and

methods). Aβ$_{1-42}$ (72 nM, applied for 40 min) evoked an increase in ROS level that was suppressed by the presence of SOD1 (Fig. 3, A and B). Previous work has suggested that ROS can be generated in response to Aβ by resident microglia (34) or perivascular macrophages (35), but the cells showing the brightest oxidized dihydroethidium fluorescence were located on capillaries, had the morphology of pericytes, and could be labeled for the proteoglycan NG2 (found on pericytes) but not for the immune cell marker Iba1 (ionized calcium-binding adaptor molecule 1) (Fig. 3C), implying that they are pericytes. The ROS signal generated in regions of interest placed over the nuclei of NG2-expressing cells on capillaries (pericytes), or of Iba1-labeled immune cells, was quantified in six image stacks (one stack per slice) from slices not exposed to Aβ (containing a total of 128 pericytes and 238 Iba1-labeled cells) and eight stacks from slices exposed to Aβ (containing 171 pericytes and 270 Iba1-labeled cells). Aβ increased ROS production in pericytes by a factor of 7.28 ($P = 0.001$) and in immune (Iba1-expressing) cells by a factor of 1.76 ($P = 0.05$). Taking into account the different numbers and basal ROS production of pericytes and immune cells revealed that Aβ evoked more total ROS generation by pericytes than by immune cells by a factor of 6.4 (Fig. 3D). This is consistent with the data above (Fig. 2, F and G) and suggests that NOX4 in pericytes (27–29) is the main generator of the ROS involved in constricting capillaries early in the response to Aβ.

To confirm that both pericytes and microglia generate ROS in response to Aβ, in brain slices we fluorescently imaged the level of reduced glutathione (GSH; see materials and methods), which is consumed as it scavenges ROS. Aβ (72 nM for 40 min) reduced the GSH level in pericytes by 20% and in microglia by 55% (fig. S4; $P = 0.014$ and $P = 2 \times 10^{-29}$, respectively). These changes cannot be converted to ROS synthesis rates because they will be affected by GSH regeneration rate, which may differ in microglia and in pericytes.

Pericytes constrict capillaries in human cognitive decline patients with Aβ deposition

Because acute exposure to Aβ cannot mimic the slow increase that occurs over decades in human AD patients, we studied rapidly fixed brain cortical biopsy tissue from living patients being investigated for cognitive decline of unknown cause (see materials and methods for demographics, biopsy, and tissue-processing details). Tissue sections were labeled with antibodies recognizing residues 8 to 17 of Aβ and PDGFRβ (Fig. 4, A and B, bottom and top, respectively). Of 13 patients, 7 turned out to have Aβ deposition and 6 did not. Pericytes were readily identifiable from their PDGFRβ labeling. Averaging over 120 to 140 adjacent fields of view (400 μm square in size, randomly placed on each section as a 5 × 4 grid of squares) in tissue from the two types of patient, with the experimenter blinded to the occurrence of Aβ deposition (viewing only the PDGFRβ image
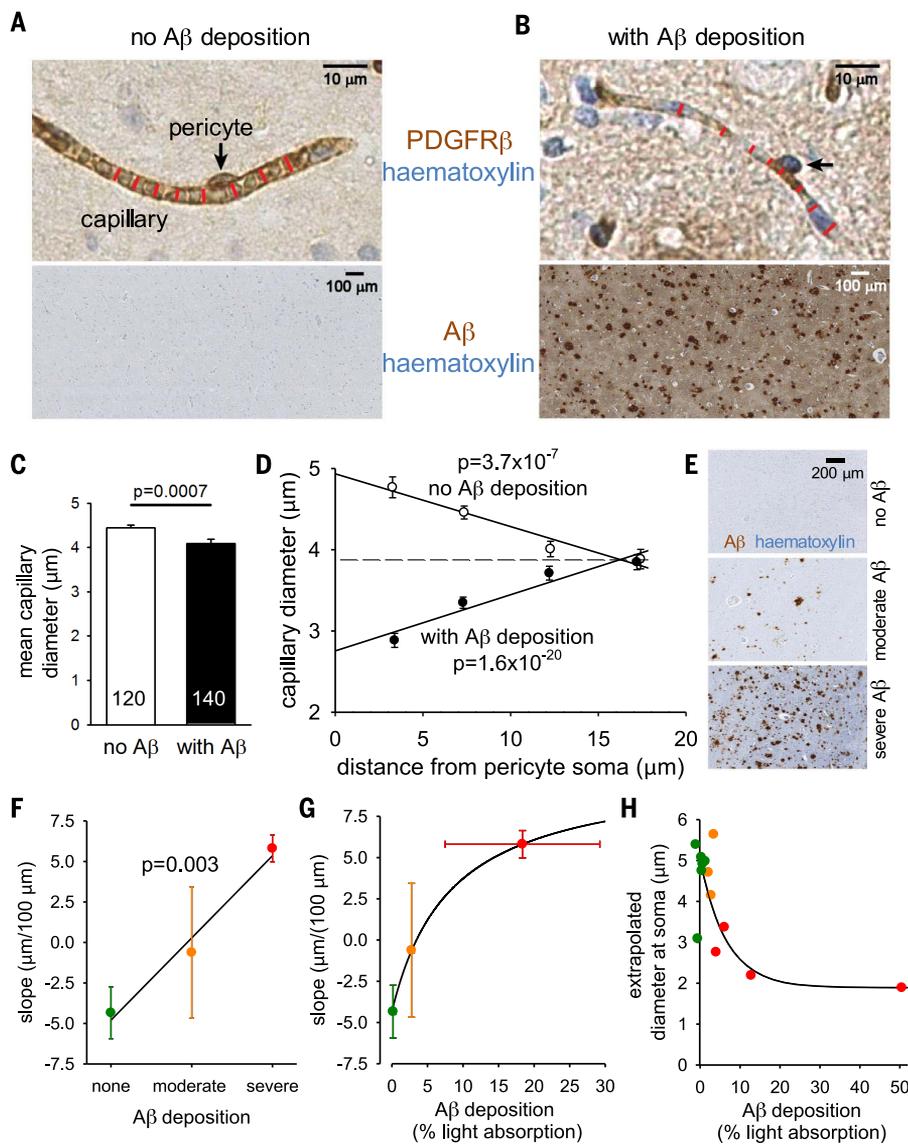
Fig. 4. Pericyte-mediated capillary constriction occurs in humans with Aβ deposits. (**A** and **B**) Specimen images of human cortical biopsies, labeled for PDGFRβ (brown in top panels) to show pericytes (arrows), from patients lacking (A) or exhibiting (B) Aβ deposits (brown in bottom panels, hematoxylin counterstain in blue). Red lines indicate capillary diameter. (**C**) Mean (± SEM) diameter of capillaries in patients lacking (3921 diameters measured) or exhibiting (5121 diameters measured) Aβ deposits (numbers of images analyzed shown on bars). (**D**) Dependence of capillary diameter on distance from a visible pericyte soma (in 5-μm bins from 0 to 20 μm, plotted at the mean distance for each bin) for patients lacking or exhibiting Aβ deposits (moderate and severe Aβ deposition pooled together). *P* values assess whether slope of regression line is significantly different from zero. (**E**) Examples of Aβ labeling assessed by the neuropathologist as absent, moderate, or severe. (**F**) Slope of regression lines as in (D) plotted as a function of neuropathologist-rated parenchymal Aβ load for each biopsy (*n* = 6 biopsies for none, *n* = 3 for moderate, *n* = 4 for severe). *P* value compares slope of line with zero. (**G**) Slope of regression lines as in (D) plotted as a function of severity of Aβ deposition measured optically for each biopsy, with subjects grouped by color [defined in (F)] as classified by the neuropathologist. (**H**) Dependence of extrapolated diameter at soma [as in (D)] on severity of Aβ deposition measured optically for each biopsy, with subject points colored as classified by the neuropathologist [defined in (F)]. Lines through data in (F) to (H) show the trends in the data.

related, we plotted the capillary diameter measurements as a function of the distance from the nearest PDGFRβ-labeled pericyte soma (see materials and methods). In patients with no detectable Aβ deposition, the capillary diameter increased at locations near pericyte somata relative to locations far from the somata (~25% larger, slope of line is significantly less than zero, *P* = 3.7 × 10⁻⁷ for 813 data points from six such patients; Fig. 4D). A similar increase in capillary diameter near somata was previously found in rodent brain capillaries in vivo (*19*) and was attributed to the presence of the soma inducing more growth of the endothelial tube. In contrast, in patients with Aβ deposition, the capillary diameter was significantly reduced near the pericyte somata relative to locations distant from the somata (Fig. 4D; ~30% smaller, slope of line is significantly greater than zero, *P* = 1.6 × 10⁻²⁰ for 1313 data points from seven patients), as expected if pericytes cause the capillary constriction by contracting their circumferential processes that are mainly located near their somata. The data shown in Fig. 4D are averaged over all measured pericytes and capillaries (and thus include pericytes on higher–branch order vessels that may be less contractile). For a fixed blood pressure applied at the pial vessels, this average constriction is predicted to reduce flow by ~50% versus what it would be in the absence of constriction (see materials and methods), which is similar to the 42% decrease observed in the gray matter in patients with AD (*3*).

The pericyte soma-specific location of the constriction (Fig. 4D) is consistent with the distribution of circumferential processes relative to pericyte somata and the fact that exogenous vasoconstrictors constrict capillaries specifically at pericyte locations (fig. S3) (*18*). These data, and the fact that no other cells on capillaries show contractile activity (*18*), imply that it is pericytes that constrict capillaries in human patients depositing Aβ.

Pericyte constriction of human capillaries increases with Aβ load

The subjects were classified by neuropathologists assessing the Aβ-labeled biopsies as having "no Aβ deposition," "moderate Aβ deposition," or "severe Aβ deposition" in the parenchyma (as diffuse deposits and/or as plaques with central amyloid cores; Fig. 4E). The mean slope for individual patients, from graphs like those in Fig. 4D, for six patients with no Aβ deposition, three patients with moderate deposition, and four patients with severe deposition showed a progressive change from negative (implying a larger capillary diameter at the soma) to positive (implying a smaller diameter at the soma) as the severity of the Aβ deposition increased (Fig. 4F; *P* = 0.003 compared with a relationship with zero slope). This further supports the idea that Aβ is the cause of the capillary constriction.

To quantify Aβ levels more rigorously, we measured light absorption by the peroxidase product generated by the Aβ antibody, in the region where the vessel diameters were measured

channel), we found no significant change in capillary density (12% larger in subjects depositing Aβ, *P* = 0.56; see materials and methods). However, the mean capillary diameter was reduced by 8.1% (*P* = 0.0007) in the patients with Aβ de-

position (5121 diameters measured) relative to those without Aβ deposition (3921 diameters measured; Fig. 4C).

To assess whether this diameter reduction was a nonspecific effect of AD, or was pericyte-

Fig. 5. Capillaries, but not arterioles or venules, are constricted in AD mice. (**A**) Specimen images (taken through the dura) of blood vessels in the somatosensory neocortex of wild-type (WT) and homozygous AD (APP^{NL-G-F}) NG2-DsRed mice, with FITC-albumin (green) in the blood (pericytes are labeled red). (**B**) Examples of single neocortical capillaries and pericytes, showing a larger diameter at the pericyte soma in a WT mouse and constriction of a capillary at the pericyte soma in an AD mouse. (**C**) Images of neocortex labeled for nuclei (DAPI, blue) and for amyloid plaques (green, 82E1 antibody). (**D**) Mean (± SEM) capillary diameter in neocortical layers I to IV in three WT mice (2131 diameters measured; measurements on same capillary were averaged) and four AD mice (1403 diameters measured). Numbers of capillaries are shown on bars. (**E**) Mean neocortical capillary diameter at pericyte somata in three WT and four AD mice (numbers of pericytes on bars). (**F**) Plot of neocortical capillary diameter as a function of distance from pericyte somata shows a smaller diameter at the soma in AD mice and a larger diameter in WT mice (compare with Fig. 4D; each WT mouse studied showed a negative slope for this relationship, and each AD mouse showed a positive slope). (**G**) Plots as in (F) but for the cerebellum, which lacks amyloid plaques, show no constriction near the pericyte somata in the AD mice (regression line is a fit to all data from three WT and three APP mice). (**H**) Mean diameter of neocortical penetrating arterioles and venules in WT and AD mice. Numbers of vessels are shown on bars. Diameters were assessed at depths that did not differ significantly: 158.4 ± 6.7 μm and 131.9 ± 5.0 μm (P = 0.23, Mann-Whitney test) for neocortical capillaries, 142 ± 26 μm and 137 ± 21 μm (P = 0.88) for arterioles, and 85 ± 15 μm and 89 ± 9 μm (P = 0.81) for venules, in WT and AD mice, respectively.

in each biopsy (see materials and methods; although this measure of Aβ may largely reflect the presence of plaques, it is likely that the soluble Aβ concentration correlates with plaque load). Plotting the slopes of graphs like those in Fig. 4D, for each biopsy, as a function of the amount of Aβ deposition again showed a monotonic progression from a negative slope to a positive slope as Aβ deposition increased, but with the change of slope occurring more strongly at low levels of Aβ deposition (Fig. 4G). Similarly, plotting the value of the capillary diameter at the pericyte soma for each biopsy (extrapolated from a straight line fit as in Fig. 4D) as a function of Aβ deposition showed that the diameter was reduced strongly by low levels of Aβ, with smaller increments of

constriction as deposition increased (Fig. 4H). This presumably reflects the dose-response curve of Fig. 2D (although it could also reflect increased Aβ production when blood flow is less).

Pericytes constrict capillaries in vivo in AD mice

To confirm that pericytes constrict capillaries in vivo in AD (i.e., that the constriction seen in human biopsy tissue was not an artifact of fixing the tissue), and to provide a possible framework for future testing of drugs to prevent this constriction, we used in vivo two-photon imaging of layers I to IV of the somatosensory cortex (Fig. 5, A and B) in a mouse model of AD, in which amyloid precursor protein (APP) with a

humanized Aβ region with three AD-related mutations (App^{NL-G-F}) is knocked in (see materials and methods). Comparing four homozygous AD mice and three wild-type mice [age range, postnatal day 119 (P119) to P143, when the AD mice already show plaques; Fig. 5C] revealed that, as in human subjects with and without Aβ deposition, in AD mice the mean capillary diameter was less (Fig. 5D, P = 1.7 × 10^{-9}), and the diameter at pericyte somata was more strongly reduced (Fig. 5E, P = 1.6 × 10^{-17}). A plot of capillary diameter as a function of distance from pericyte somata showed a dilation at the soma in wild-type mice, but a constriction in the AD mice (Fig. 5F), relative to the diameter midway between somata (compare with Fig. 4D).

To check whether capillary constriction was present throughout the brain of AD mice, or occurred only where Aβ levels rise, we imaged capillaries in vivo in the cerebellum—an area that is relatively spared of amyloid plaque pathology in humans, and that had no plaques in our AD mice at P120 to P140 (fig. S5), suggesting lower levels of Aβ oligomers. In the cerebellum, both wild-type and AD mice (n = 3 each) showed a larger capillary diameter near pericyte somata (Fig. 5G; P = 0.002), with no evidence for a constriction in the AD mice. Thus, capillary constriction is associated with Aβ production.

Exogenous Aβ has been reported to constrict isolated penetrating arterioles (12) but, at the endogenous level of Aβ produced in the AD mice, arterioles (and venules) were not constricted (Fig. 5H). This may reflect a different response of pericytes and of arteriolar smooth muscle cells to the ET released by Aβ (fig. S6). The lack of arteriole constriction that we observed in the AD mice (Fig. 5H) suggests that capillary constriction is the cause of the decrease in cerebral blood flow that occurs in early AD (1).

Hypoxia is increased in the AD cortex

Our measured capillary constrictions are predicted to decrease cerebral blood flow significantly in AD (see above and materials and methods), as has been observed in human patients and AD mice (1, 17, 21). Consistent with this, hypoxic tissue labeling by pimonidazole (hypoxyprobe) was increased significantly in vivo in the AD mice (fig. S7).

Reversal of Aβ-evoked capillary constriction

Prevention or reversal of Aβ-evoked capillary constriction and tissue hypoxia could be a promising therapy in early AD. In brain slices, we investigated two strategies to achieve this (fig. S8), assuming it were possible to target drugs specifically to central nervous system (CNS) capillaries. The first strategy involved combined block of the ROS generator NOX4 (with 0.45 μM GKT137831; Fig. 2F) and of the downstream constricting ET_A receptor (with 1 μM BQ-123; Fig. 2E). This prevented further constriction evoked by Aβ (P = 0.027) but did not reverse the capillary diameter to its baseline value on a 1-hour time scale (Fig. 6A). The second strategy used C-type natriuretic peptide (CNP), which can reverse ET-mediated effects (36) by blocking Ca^{2+} release from internal stores and activating myosin light chain phosphatase (fig. S8). Remarkably, CNP (100 nM) reversed the Aβ-evoked capillary constriction (P = 0.029; Fig. 6A).

Discussion

Genetic evidence strongly implicates Aβ in triggering neuronal damage and cognitive decline in Alzheimer's disease, yet the first change in AD is a decrease of cerebral blood flow (1). Our data make five contributions to understanding the vascular effects of Aβ and their role in Alzheimer's disease: (i) Aβ constricts human and rodent capillaries by acting on pericytes; (ii) the mechanism
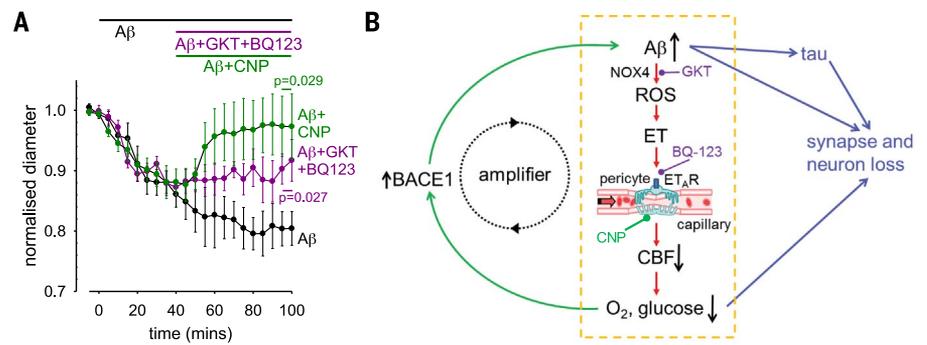
Fig. 6. Aβ effects on capillaries may amplify the onset of AD and are reversible. (**A**) Applying GKT137831 (0.45 μM) to block NOX4 and BQ-123 (1 nM) to block ET_A receptors, or applying C-type natriuretic peptide (CNP, 100 nM; see fig. S8), significantly reduced the constriction evoked by Aβ (72 nM, P = 0.027 and 0.029, respectively, corrected for multiple comparisons; data are means ± SEM). (**B**) Summary of our results and their implications. Our data reveal the pathway within the yellow dashed box. Aβ oligomers activate NOX4 in pericytes to generate ROS. These in turn release, or potentiate the constricting effects of, endothelin-1, which acts via ET_A receptors on pericytes on capillaries—the locus (16) of the largest component of vascular resistance within the brain parenchyma. Capillary constriction decreases cerebral blood flow and hence the supply of oxygen and glucose to the brain. Green arrows at the left show that this increases the production of Aβ, in part by up-regulating (13, 14) the expression of BACE1, thus forming an amplifying positive feedback loop. Blue arrows at the right show that a rise in Aβ concentration (directly, via downstream tau production, or via the decrease in oxygen and glucose supply) leads to the loss of synapses and neurons. Potential sites for therapeutic intervention are highlighted at the stages of ROS production by NOX4 (GKT), endothelin receptors (BQ-123), and CNP receptors (see also fig. S8).

of this constriction involves ROS generation and ET release; (iii) in rapidly fixed biopsies from living human patients with Aβ deposition and cognitive decline, cortical capillaries are constricted by 30% at pericyte locations, which is sufficient to produce a major reduction of cerebral blood flow; (iv) in vivo, in a rodent model of AD, capillaries are constricted by pericytes; and (v) it is in principle possible to reverse the Aβ-evoked capillary constriction. Together, these data imply that the reduction in cerebral blood flow that occurs early in AD results from Aβ-evoked pericyte-mediated constriction of the cerebral capillary bed (Fig. 6B).

At low nanomolar concentrations, exogenous soluble $Aβ_{1-42}$ oligomers evoke a constriction of human and rat cortical capillaries, which is mediated by pericytes. Capillaries are the site in the cortical vasculature where most of the resistance to flow is located (16), and so may be the major site where Aβ produced within the brain can produce vessel diameter changes that reduce cerebral blood flow. In rodents, the capillary constriction was the result of Aβ evoking the generation in pericytes and microglia of ROS, which evoked a release of ET that acted via ET_A receptors to make pericytes constrict the capillaries. We assume that the ET_A receptors involved are located on the pericytes themselves, because ET raised the $[Ca^{2+}]_i$ in pericytes, but we cannot rule out the possibility that they are on a different cell type. The EC_{50} for the action of $Aβ_{1-42}$, 4.7 nM, is comparable to the concentration of soluble Aβ found in the human AD brain [6 nM, from table 1 of (37); note that this brain concentration is higher than the level found in the CSF, which falls during the development of AD

as plaques are formed]. Thus, wherever Aβ is produced, or can diffuse, in the AD brain, we would expect all contractile pericytes in that region to constrict capillaries. Indeed, our live human biopsy and in vivo mouse imaging data show that the endogenous level of Aβ reached in AD is sufficient to constrict capillaries. However, some aging humans accumulate Aβ and yet do not develop AD; future work could examine whether, in such people, compensation for the vasoconstricting effects of Aβ develops, such as an up-regulation of vasodilatory mechanisms.

Throughout this work, pericytes were identified by their morphology (spatially isolated cells located outside capillaries) as confirmed by IB_4 labeling, or by antibody labeling for their characteristic marker PDGFRβ, or by expression of dsRed under the NG2 promoter. Although arterioles (recognized as being surrounded by rings of abutting smooth muscle cells) have also been reported to be constricted by exogenous Aβ (12), in AD mice we found no constriction of arterioles. This may be because, at the ET level reached during AD pathology, ET constricts capillaries but has opposing dilating and constricting effects on arterioles, mediated by different types of ET receptor, which may approximately cancel out. Further work assessing the level of Aβ reached in the AD mice, and the relative affinity of the constricting ET_A and dilating ET_B receptors, will be needed to test this idea.

Three results demonstrate that the effects of Aβ on pericytes that we have demonstrated are pathologically relevant in AD. First, analyzing the diameter of capillaries in biopsies from living human patients with cognitive decline, who either had or lacked Aβ deposition, showed that

Alzheimer's pathology leads to capillary constriction specifically at pericytes. Second, the magnitude of the capillary constriction in human dementia patients increased with the severity of Aβ deposition and is predicted to produce a decrease of cerebral blood flow (~50%) similar to the 42% seen in AD patients (*3*). Capillary constriction by pericytes may explain why some capillaries become occluded by neutrophils in AD (*38*), but neutrophil block of 2% of capillaries, as observed, was predicted to reduce blood flow by only 5% (*38*). Finally, in a mouse model of AD, in vivo imaging showed that cerebral capillaries were constricted at pericyte locations, whereas arterioles and venules were unaffected.

Both the reduction of basal blood flow produced by Aβ and a reduction in the blood flow increase normally produced by neuronal activity (*39*), which may also reflect the constricting action of Aβ on pericytes, will decrease the energy supply to the brain. This in turn increases Aβ production by up-regulating β-amyloid–converting enzyme (BACE1, also called β-secretase 1) (*13*, *14*). Consequently, the pericyte-mediated capillary constriction evoked by Aβ may act as an amplifying mechanism in a positive feedback loop (Fig. 6B), increasing the levels of Aβ and downstream hyperphosphorylated tau, which ultimately lead to the loss of synapses and neurons.

These data suggest several potential therapeutic approaches for early AD, based on the mechanisms generating pericyte constriction. Aβ-evoked generation of ROS by NOX4 in pericytes might be targeted. Indeed, overexpression of SOD1 in APP-overexpressing mice abolishes the lethal effects of the APP overexpression (*26*, *40*). Another approach might be to try to reduce ET release [presumably from brain cells expressing ET strongly, i.e., endothelial cells, microglia, or pericytes (*28*, *29*)] or to block the effects of ET on its ET_A receptors on CNS pericytes. In a proof-of-concept experiment, a combination of a NOX4 blocker and an ET_A blocker prevented further Aβ-evoked constriction (and could conceivably reverse the existing constriction given sufficient time), whereas CNP, which acts via two separate pathways downstream of ET (fig. S8), was able to reverse the constriction in the maintained presence of Aβ. These therapeutic approaches could be tested by targeting drugs to CNS pericytes in the mouse model of AD, which also shows the pericyte-mediated constriction of capillaries. Finally, our scheme (Fig. 6B) prompts the question of what fraction of the damage to synapses and neurons in AD reflects direct actions of Aβ and downstream tau, and what fraction is a consequence of the decrease of energy supply that Aβ produces by constricting capillaries.

Materials and methods
Human brain slices
The work on fresh living human brain tissue received ethical approval from the National Health Service (REC number 15/NW/0568) and all patients gave informed consent. During neurosurgical operations for tumor treatment, apparently normal cortical tissue that was removed

(to gain access to the tumor), which would otherwise have been discarded, was placed in ice-cold brain slicing solution containing 93 mM *N*-methyl-D-glucamine (NMDG) chloride, 2.5 mM KCl, 30 mM NaHCO₃, 10 mM MgCl₂, 1.2 mM NaH₂PO₄, 25 mM glucose, 0.5 mM CaCl₂, 20 mM HEPES, 5 mM Na ascorbate, 3 mM Na pyruvate, and 1 mM kynurenic acid (to block glutamate receptors, so as to prevent excitotoxic damage to neurons during the slicing; the experimental solution lacked kynurenic acid, as described below). This solution was oxygenated by gassing with 95% O_2/5% CO_2 and transported in less than 15 min to the laboratory. Tissue was cut into 200-μm sections and the slices were incubated at 34°C in the same solution for 10 min, and then incubated at room temperature until used in experiments in a similar solution (*41*) with the NMDG-Cl, MgCl₂, and CaCl₂ replaced by 92 mM NaCl, 1 mM MgCl₂, and 2 mM CaCl₂. Each patient's tissue typically generated ~2 brain slices. When sufficient tissue was present, histological examination of the slices using hematoxylin and eosin by neuropathologists was used to assess tumor infiltration into the nominally normal tissue. This revealed that some slices showed no infiltration by the tumor, whereas others did. Aβ was applied only to slices that showed no tumor infiltration. Pericyte responses to noradrenaline and glutamate as documented in Fig. 1 were observed whether or not there was tumor infiltration.

Rodent brain slices
Experiments used P21 Sprague-Dawley rats or transgenic mice (as described below) of either sex. All animal procedures were carried out in accordance with EU and UK regulations. Cerebral cortical slices (300 μm thick) were prepared (*18*) and stored as for human slices.

Extracellular solution
Human and rodent brain slices were superfused at 3 to 4 ml/min with aCSF solution containing 124 mM NaCl, 2.5 mM KCl, 26 mM NaHCO₃, 1 mM MgCl₂, 1 mM NaH₂PO₄, 10 mM glucose, 2 mM CaCl₂, and 1 mM Na-ascorbate. This solution was gassed with 20% O_2/75% N_2/5% CO_2, which produces a physiological level of oxygen in the slice near the capillaries being imaged (*19*). Mechanism-blocking drugs were superfused for 5 to 15 min before applying Aβ or ET.

Imaging capillaries in brain slices
Healthy capillaries [<10 μm in diameter, mean diameter 5.61 ± 0.03 μm (*n* = 299) in rat and 5.08 ± 0.33 μm (*n* = 12) in human, with no rings of arteriolar smooth muscle around them] were selected as described (*41*) and regions of them were imaged, which were in focus in a single image plane over at least 30 μm along the length of a capillary and which exhibited a candidate pericyte with a bump-on-a-log morphology (Figs. 1E and 2A). A CCD camera was used to capture images 100 μm square during superfusion of drugs. An analyst blinded to the time and identity of drug application measured capillary diameter from the resulting movies by placing a line across

the lumen on magnified images using Metamorph software. In some experiments, pericytes were identified prior to imaging by incubating slices for 30 min in IB_4 (10 μg/ml) conjugated to Alexa 488 or 568 (ThermoFisher I21411 or 121412), which binds to α-D-galactose residues in the basement membrane generated by pericytes and endothelial cells, and outlines pericytes (*41*). This also allowed two-photon imaging (using a Zeiss LSM710 microscope, excitation wavelength 800 nm) of the endothelial tube and the pericytes on it (Fig. 2B).

Oligomerizing Aβ and assessing the form and concentration of Aβ applied
The method used to generate oligomeric Aβ preparations was modified from that previously described (*42*). Synthetic Aβ₁₋₄₂ (Bachem H-1368.1000), Aβ₁₋₄₀ (Bachem H-1194.1000), and scrambled Aβ₁₋₄₂ (Bachem H-7406.1000) were suspended in 1,1,1,3,3,3-hexafluoro-2-propanol (HFIP; 52527, Sigma) at 1 mM, vortexed to obtain a homogeneous solution, and aliquoted to microcentrifuge tubes. The HFIP was removed by overnight evaporation and the Aβ was completely lyophilized via a Speed-Vac. The peptide films were stored desiccated at –80°C until further processed (within 2 weeks). The peptide films were then resuspended at a nominal 5 mM in DMSO, bath-sonicated for 10 min, and vortexed for 30 s. To form Aβ oligomers, this solution was diluted to a nominal 100 μM with phosphate-buffered saline (PBS), vortexed for 15 to 30 s, and incubated at 4°C for 24 hours. Immediately before use, the oligomeric preparations were centrifuged at 14,000*g* for 10 min at 4°C (to remove any fibrils that might be present) and the supernatants were further diluted to the final experimental concentrations (quantified below) with extracellular solution.

Quantification of Aβ peptide concentration was performed using a Pierce BCA protein assay kit (ThermoFisher 23227), calibrated against a known concentration of bovine serum albumin, taking into account the different chromophoric development of albumin and Aβ peptides by multiplying by a factor of 1.51 (*43*, *44*). This showed that the amount of the molecule remaining as soluble monomers and oligomers (i.e., not undissolved or removed as fibrils) was 28.7 ± 2.9% (*n* = 4) of the nominal concentration added for Aβ₁₋₄₂, 39.9 ± 1.5% (*n* = 4) for Aβ₁₋₄₀, and 43.6 ± 2.3% (*n* = 3) for scrambled Aβ₁₋₄₂. Concentrations stated in the text have been corrected for these factors and are given based on the monomeric molecular weight. It was not possible to make pure monomeric preparations of Aβ₁₋₄₂ or Aβ₁₋₄₀.

The Aβ oligomeric preparations were analyzed via SDS-PAGE using 10 to 20% Tris-glycine gels (EC61352BOX, Invitrogen). Samples of Aβ peptides (50 μg) were added to Tris-glycine SDS sample buffer (LC2676, Invitrogen). Equal volumes of each sample (10 μl) were loaded onto gels along with SeeBluePlus2 (Invitrogen) prestained molecular weight markers and electrophoretically separated at 100 V. Gels were stained for total protein using a SilverXpress Silver Staining kit (LC6100, Invitrogen) according to the

manufacturer's protocol. $A\beta_{1-42}$ and $A\beta_{1-40}$ formed monomers and oligomers, whereas scrambled $A\beta_{1-42}$ formed mainly monomers (Fig. 1G). Using densitometry, we estimated that for Fig. 1G the percentages of $A\beta_{1-42}$, $A\beta_{1-40}$, and scrambled $A\beta_{1-42}$ present as monomers (defined as molecular weight 2.5 to 6.5 kDa) were 48%, 39%, and 89%, respectively; the percentages as dimers (MW 6.5 to 11.5 kDa) were 11%, 46%, and 11%; the percentages as trimers (MW 11.5 to 15.5 kDa) were 22%, 6%, and 0%; and the percentages as tetramers (MW 15.5 to 20.5 kDa) were 19%, 4%, and 0%. Thus, the measured EC_{50} of 4.7 nM for the effect of $A\beta_{1-42}$ on constriction in Fig. 1D, which was calculated based on the monomeric molecular weight, would become approximately 4.7 × 0.19 = 0.9 nM if only the tetramer was active.

Immunohistochemistry of non-biopsy tissue

Human and rat brain slices were fixed in 4% paraformaldehyde (PFA) for 1 hour, washed three times in PBS, then blocked in 10% goat serum/0.5% Triton X-100 in PBS. Primary antibodies for PDGFRβ (Santa Cruz, sc432, 1:200) or α-SMA (Santa Cruz, CGA7, 1:200) or Aβ (IBL, 82E1, 1:500) were applied overnight, followed (after washing in PBS) by application overnight of Alexa Fluor 647 or 633 conjugated secondary antibodies (ThermoFisher, A-21245, A-21070, A-21050, 2 μg/ml). Slices were then washed once in PBS containing DAPI nuclear stain (1:50,000) for 10 min and then washed again in PBS. After mounting, slices were imaged on a Zeiss LSM700 confocal microscope.

Imaging pericyte [Ca²⁺]ᵢ

Experiments were carried out on acute cortical brain slices from P44 to P88 mice, of either sex, generated by crossing tamoxifen-inducible NG2-Cre^{ERT2} mice (45) with floxed GCaMP5G-IRES-tdTomato mice (JAX 024477). Coexpression of the genetically encoded Ca^{2+} indicator GCaMP5G and the morphological marker tdTomato (driven by the CAG promoter after Cre-mediated recombination) was induced by oral gavage of tamoxifen (1 mg per 10 g body weight) for four consecutive days (starting from P23). Brain slices (300 μm thick) were prepared from 21 days after the first tamoxifen administration, as described above for human and rat brain slices. Cortical capillary pericytes, identified in the tdTomato channel from their bump-on-a-log somatic morphology and processes wrapped around capillaries, were imaged using a two-photon microscope (Zeiss LSM 710 or 780) with the two-photon laser (Ti: sapphire Mai Tai DeepSee, Spectra Physics) tuned to 940 nm. Images were acquired with a 20×/1.0 NA water immersion objective (W Plan-Apochromat, Zeiss). Laser power was 5 to 20 mW in the focal plane. Emitted fluorescence was spectrally divided by a 555-nm dichroic mirror and collected by GaAsP detectors. Two-photon image stacks (50 to 200 μm × 50 to 200 μm × 20 to 40 μm; 150 to 300 nm pixel size, 2 μm z-step size, 1.58 to 2.55 μs pixel dwell time) were acquired every 30 s and processed using FIJI (ImageJ). Image stacks were first projected at

maximum intensity in the z-dimension, and both channels were co-registered to correct for movement artifacts using the FIJI plugin Multistackreg. Percentage changes in the GCaMP5G fluorescence of regions of interest (ROIs) drawn around pericyte somata were calculated. Oligodendrocyte precursor cells (OPCs), identified on the basis of a starlike morphology and weaker baseline fluorescence, and arteriolar smooth muscle cells were excluded from the analysis.

Assessing pericyte death

This was carried out as described (19). Briefly, brain slices (250 μm thick) were incubated at 36° ± 1°C in a multiwell plate, with 95% O_2/5% CO_2 blown gently at the surface, in aCSF, or aCSF with oligomerized $A\beta_{1-42}$ or ET added. All extracellular solutions contained IB_4 (41) to label the basement membrane (ThermoFisher I21411, 10 μg/ml), and hence to label pericytes that are enveloped by this (Fig. 1B), and 7.5 μM propidium iodide to label cells with membranes that had become nonspecifically permeable (19). After 3 hours of incubation, slices were fixed in 4% PFA for 2 hours, washed three times with PBS for 15 min each, mounted in DAKO medium, and imaged on a confocal microscope. To avoid counting cells killed by the slicing procedure, quantification of the percentage of pericytes that were dead excluded cells within 20 μm of the slice surface.

Imaging ROS production

Cellular production of ROS in brain slices was visualized through the O_2•-specific oxidation of dihydroethidium to ethidium, which binds to the DNA and RNA of O_2•-producing cells (46). Rat cortical slices (250 μm thick) were incubated in aCSF or in aCSF containing $A\beta_{1-42}$ (72 nM) or $A\beta_{1-42}$ + SOD1 (150 units/ml) at 34°C. Dihydroethidium (DHE, 8 μM, Cayman, 104821) was added to all solutions immediately before use to avoid auto-oxidation of the dye. No preincubation with DHE was used, so as to limit the intracellular accumulation of oxidized product. After 40 min, the slices were quickly rinsed in PBS, mounted, and immediately imaged using a confocal microscope. A single image stack was acquired at the middle of each slice and for Fig. 3B the fluorescence intensity of the maximum intensity projections was measured using ImageJ. For establishing the identity of ROS-producing cells, slices were fixed in 4% PFA for 20 min and immunostained for NG2 (Millipore AB5320, 1:200) and Iba1 (Synaptic Systems 234006, 1:200). Alexa 488-IB_4 (ThermoFisher I21411, 10 μg/ml) was added with the secondary antibodies to also label blood vessels. In maximum intensity projections of z-stacks, ROIs were then drawn around the nuclei of pericytes (NG2-expressing cells on capillaries) and Iba1-expressing immune cells (microglia and perivascular macrophages) and the DHE signal within each ROI was measured in ImageJ. For each z-stack, a mean intensity per pericyte or Iba1-labeled cell, and the total intensity per population of pericytes or Iba1-labeled cells, were calculated, and analysis was performed using the z-stack as the statistical unit.

For glutathione imaging, rat brain slices were incubated with Aβ and fixed as described above, then incubated with 10 mM N-ethylmaleimide (NEM) for 4 hours at 4°C and washed thoroughly with PBS. The sections were additionally immunolabeled with a GSH-NEM antibody (Millipore MAB3194, 1:500), which is specific to this adduct, allowing quantification of reduced glutathione after reaction with NEM (47). After confocal imaging, ROIs were drawn around the soma of IB_4-labeled pericytes and Iba1-expressing immune cells as above and the total fluorescence signal for GSH-NEM was quantified for each cell and averaged over cells.

Human biopsy data

Diagnostic brain biopsies, comprising cortex and subcortical white matter, were performed as part of routine clinical investigation at the National Hospital for Neurology and Neurosurgery, Queen Square, London, to exclude treatable causes of neurological symptoms that patients showing cognitive decline had presented with. All patients gave informed consent for the biopsy. The use of human tissue samples was licensed by the National Research Ethical Service, UK (University College London Hospitals NRES license for using human tissue samples, project ref 08/0077). The storage of human tissue was licensed by the Human Tissue Authority, UK (License #12054).

Biopsies (volume typically 1 cm³) were all from the right frontal lobe. The biopsies were fixed in 10% buffered formalin less than 30 min after the resection, for a minimum of 12 hours. The formalin-fixed tissue was dehydrated through graded alcohols and embedded in paraffin wax, from which 4-μm-thick sections were cut for routine hematoxylin and eosin staining and a panel of immunohistochemical stains. As part of the diagnostic workup, the sections were immunostained for Aβ with immunoperoxidase-labeled antibody 6F3D (DAKO, 1:50), and for this study in addition with antibody against PDGFRβ (RD systems, MAB1263, 1:20) to label pericytes. This was performed on a Roche Ventana Discovery automated staining platform following the manufacturer's guidelines, using biotinylated secondary antibodies and streptavidin-conjugated horseradish peroxidase and diaminobenzidine as the chromogen. The extent of parenchymal Aβ deposition was assessed semiquantitatively as absent, moderate, or severe by a neuropathologist. In addition, to objectively quantify Aβ deposition, the images of the immunoperoxidase label for Aβ were imported into ImageJ and split into red, green, and blue channels. Then, the light intensity in the blue channel (which gave best distinction of the immunoperoxidase label from the background tissue hematoxylin labeling) was measured in the region of the biopsy where diameters were measured, normalized by the intensity in a region of the section showing no visible Aβ label and converted to a percentage of light absorbed by the Aβ. Normalizing by the intensity in a (tissue-free) region without any tissue absorption gave values that were 5.8 ± 0.5% larger, which did not materially change the form of the

graphs. Although this measure of Aβ may largely reflect the presence of plaques, it is likely that the soluble Aβ concentration correlates with plaque load (*48*).

The mean age of patients without Aβ deposition was 50.5 ± 5.5 (*n* = 6, 4 women and 2 men), and of those with Aβ deposition was 62.1 ± 4.2 (*n* = 7, 4 women and 3 men, not significantly different, *P* = 0.11). Regressing mean capillary diameter against age from all patients, or from the patients lacking Aβ deposition, showed that there was no significant dependence on age (*P* = 0.5 and *P* = 0.82, respectively).

Images were analyzed to assess capillary diameter with the experimenter blinded to the level of Aβ deposits (i.e., viewing only the PDGFRβ channel; the condition of the tissue was sometimes worse for patients with Aβ deposition, but it was not possible to unambiguously decide whether the patient had Aβ deposition without viewing the Aβ channel). A standard 5 × 4 grid of 20 squares (each with sides 400 μm long) was superimposed on each image, and all capillaries with clearly demarcated endothelial walls visible in each square had their diameter measured. The image squares were treated as the experimental unit for statistical analysis. Analysis of the diameter as a function of distance from the nearest visible pericyte used a subset of all the measured diameters, because often no pericyte was visible on some short capillary segments. The total number of measurable capillary segments (within the 5 × 4 grid) per subject was not significantly different (*P* = 0.56) between subjects depositing Aβ (732 ± 96) and subjects not depositing Aβ (654 ± 88), suggesting no detectably greater loss of capillaries in the subjects depositing Aβ.

Experiments in vivo on AD mice

AD mice, in which APP with a humanized Aβ region containing three AD-related mutations (*App*^NL-G-F^) is knocked in (*49*) to avoid artifacts associated with overexpressing APP, were crossed with NG2-DsRed mice in which pericytes express DsRed (*19*). Mice aged ~4 months (P119 to P143, not significantly different for wild-type and AD, *P* = 0.13) were anesthetized using urethane (1.55 g/kg given in two doses 15 min apart). Adequate anesthesia was ensured by confirming the absence of a withdrawal response to a paw pinch. Body temperature was maintained at 36.8° ± 0.3°C and eyes were protected from drying by applying polyacrylic acid eye drops (Dr. Winzer Pharma). The animal was secured in a stereotaxic frame and lidocaine/prilocaine (AstraZeneca) was applied topically prior to exposing the skull. A custom-built headplate was then attached to the skull using superglue to create a sealed well filled with HEPES-buffered aCSF (140 mM NaCl, 10 mM HEPES, 2.5 mM KCl, 1 mM NaH_2PO_4, 10 mM glucose, 2 mM $CaCl_2$, and 1 mM $MgCl_2$) during imaging. A craniotomy of approximately 3 mm diameter was performed over the right primary somatosensory cortex, immediately caudal to the coronal suture and approximately 2 to 6 mm laterally from the midline, or over the right cerebellar hemisphere for imaging cerebellar vessels. The dura was left intact to reduce perturbation of the brain. During imaging, the headplate was secured under the objective on a custom-built stage.

Cortical or cerebellar vessel diameter was recorded using two-photon microscopy of the intraluminal dyes Cascade Blue dextran (MW 10 kDa, Invitrogen, D1976, 1.25 mg in 100 μl of saline given i.v.) or albumin–fluorescein isothiocyanate conjugate (FITC-albumin, Sigma, A9771, 1 mg in 100 μl of saline given retro-orbitally). Two-photon excitation was carried out using a Newport-Spectraphysics Ti:sapphire MaiTai laser pulsing at 80 MHz, and a Zeiss LSM710 microscope with a 20× water immersion objective (NA 1.0). Fluorescence was evoked using a wavelength of 920 nm for DsRed, 820 nm for FITC-albumin, and 800 nm for Cascade-Blue. The mean laser power under the objective did not exceed 35 mW. Penetrating arterioles >10 μm in size were identified by the typical ring shape of vascular smooth muscle cells expressing DsRed in NG2-DsRed (wild-type or APP^NL-G-F^) mice. Image stacks were taken in 2-μm depth increments across layers I to IV of the cortex (up to 400 μm deep from the cortical surface). To measure vessel diameter, a line was drawn in ImageJ across the vessel perpendicular to its axis and the width of the intraluminal dye fluorescence was measured, either manually or using an automated routine fitting a Gaussian function to the fluorescence profile in ImageJ and calculating the full width at quarter-maximum of the peak fluorescence intensity (which gave results insignificantly different from the manual measurement).

Assessing hypoxia in vivo with pimonidazole

Hypoxia was assessed in vivo using the Hypoxyprobe-Plus (HP2-100, Hypoxyprobe Inc.) kit following the manufacturer's instructions. After anesthesia induction with 3% isoflurane in air, animals were switched to 1.5% isoflurane in air and pimonidazole HCl (60 mg/kg) was injected intraperitoneally. Four hours after pimonidazole injection, animals were transferred to urethane anesthesia (1.55 g/kg) and killed by perfusion fixation. Brains were extracted and kept in paraformaldehyde for 24 hours prior to sectioning for immunohistochemistry using the FITC-conjugated antibody provided in the kit, which recognizes conjugates of pimonidazole with protein SH groups in hypoxic cells.

Statistics

Data are presented as means ± SEM. Data normality was assessed with Shapiro-Wilk or D'Agostino-Pearson omnibus tests. Comparisons of normally distributed data were made using two-tailed Student *t* tests. Equality of variance was assessed with an F test, and heteroscedastic *t* tests were used if needed. Data that were not normally distributed were analyzed with Mann-Whitney tests. *P* values were corrected for multiple comparisons using a procedure equivalent to the Holm-Bonferroni method (for *N* comparisons, the most significant *P* value is multiplied by *N*, the 2nd most significant by *N* – 1, the 3rd most significant by *N* – 2, etc.; corrected *P* values are significant if they are less than 0.05). Assessment of whether the slope of linear regressions differed significantly from zero was obtained using the *t* statistic for the slope. *P* values comparing vessel diameters in the absence and presence of drugs were calculated for the last data point in each graph shown, or for an exposure time of 45 to 60 min if no graph is shown. An estimate of the sample size needed for a typical experiment is as follows: For a control response of 100%, a response standard deviation of 10%, a response in a drug of 70% (30% inhibition), a power of 80% and *P* < 0.05, fewer than six vessels are needed in each of the control and drug groups (www.biomath.info/power/ttest.htm). The exact numbers depend on the drug effect size and standard error of the data.

Calculation of effect of vessel constriction on flow

We assume that pericytes are regularly spaced on capillaries at an interval of 2*L*. For flow governed by Poiseuille's law, the resistance of a segment of capillary of length *L* (from a pericyte soma to midway between two pericytes) and radius r_1 is given by

$$\frac{kL}{r_1^4}$$

where *k* is a constant. If Aβ-induced pericyte contraction reduces the capillary diameter from a value of r_1 at the midpoint between pericytes to r_2 near the pericyte soma (see Fig. 4, A, B, and D), then, if this reduction is linear with distance, the resistance of the capillary segment from the soma to the midpoint is given by

$$\frac{kL(r_1^2 + r_1 r_2 + r_2^2)}{3r_1^3 r_2^3}$$

so the factor by which the resistance is altered (relative to that with a uniform diameter r_1) is

$$\frac{\left[1 + \frac{r_1}{r_2} + \left(\frac{r_1}{r_2}\right)^2\right]\frac{r_1}{r_2}}{3}$$

Thus, with Aβ deposition, the 30% pericyte constriction reported at pericyte somata in Fig. 4D will increase the resistance by a factor of 2.1 relative to a situation with the capillary having a uniform diameter equal to that measured far from the pericyte somata (~3.9 μm in Fig. 4D), and the 27% increase in diameter at the soma in subjects without Aβ deposition will decrease the resistance to 0.63 of the value with a uniform capillary. Taking the ratio of these changes leads to the conclusion that the capillary constriction occurring with Aβ deposition will increase the capillary resistance by a factor of 3.4 (relative to the condition with no Aβ deposition). Because the capillaries provide 57% of the total vascular resistance in the brain parenchyma (*16*), and because the diameter of arterioles and venules is

not changed (Fig. 5H), it follows that if the pressure is fixed at the pial end of penetrating arterioles and venules, then cerebral blood flow will be decreased by 58%, calculated as (43% + 57%)/[43% + (3.4 × 57%)]. In reality, the flow reduction could be greater than this because Poiseuille's law does not apply for small capillary diameters for which the effective blood viscosity increases as the diameter decreases below 10 μm (*50*). Note that the data in Fig. 4 were averaged over all visible pericytes in the images, and so they already take account of the fact that the contractility of capillary pericytes decreases for higher branch orders of capillary (*19*).

REFERENCES AND NOTES

1. Y. Iturria-Medina, R. C. Sotero, P. J. Toussaint, J. M. Mateos-Pérez, A. C. Evans, Alzheimer's Disease Neuroimaging Initiative, Early role of vascular dysregulation on late-onset Alzheimer's disease based on multifactorial data-driven analysis. *Nat. Commun.* **7**, 11934 (2016). doi: 10.1038/ncomms11934; pmid: 27327500

2. S. Love, J. S. Miners, Cerebrovascular disease in ageing and Alzheimer's disease. *Acta Neuropathol.* **131**, 645–658 (2016). doi: 10.1007/s00401-015-1522-0; pmid: 26711459

3. I. Asllani et al., Multivariate and univariate analysis of continuous arterial spin labeling perfusion MRI in Alzheimer's disease. *J. Cereb. Blood Flow Metab.* **28**, 725–736 (2008). doi: 10.1038/sj.jcbfm.9600570; pmid: 17960142

4. J. Kang et al., The precursor of Alzheimer's disease amyloid A4 protein resembles a cell-surface receptor. *Nature* **325**, 733–736 (1987). doi: 10.1038/325733a0; pmid: 2881207

5. J. Hardy, D. Allsop, Amyloid deposition as the central event in the aetiology of Alzheimer's disease. *Trends Pharmacol. Sci.* **12**, 383–388 (1991). doi: 10.1016/0165-6147(91)90609-V; pmid: 1763432

6. D. J. Selkoe, The molecular pathology of Alzheimer's disease. *Neuron* **6**, 487–498 (1991). doi: 10.1016/0896-6273(91)90052-2; pmid: 1673054

7. T. Kimura, T. Hashimura, T. Miyakawa, Observations of microvessels in the brain with Alzheimer's disease by the scanning electron microscopy. *Jpn. J. Psychiatry Neurol.* **45**, 671–676 (1991). pmid: 1800815

8. J. C. de la Torre, T. Mussivan, Can disturbed brain microcirculation cause Alzheimer's disease? *Neurol. Res.* **15**, 146–153 (1993). doi: 10.1080/01616412.1993.11740127; pmid: 8103579

9. T. Thomas, G. Thomas, C. McLendon, T. Sutton, M. Mullan, β-Amyloid-mediated vasoactivity and vascular endothelial damage. *Nature* **380**, 168–171 (1996). doi: 10.1038/380168a0; pmid: 8600393

10. Z. Suo et al., Soluble Alzheimers β-amyloid constricts the cerebral vasculature in vivo. *Neurosci. Lett.* **257**, 77–80 (1998). doi: 10.1016/S0304-3940(98)00814-3; pmid: 9865931

11. R. Deane et al., RAGE mediates amyloid-β peptide transport across the blood-brain barrier and accumulation in brain. *Nat. Med.* **9**, 907–913 (2003). doi: 10.1038/nm890; pmid: 12808450

12. H. H. Dietrich, C. Xiang, B. H. Han, G. J. Zipfel, D. M. Holtzman, Soluble amyloid-β, effect on cerebral arteriolar regulation and vascular cells. *Mol. Neurodegener.* **5**, 15 (2010). doi: 10.1186/1750-1326-5-15; pmid: 20388225

13. X. Sun et al., Hypoxia facilitates Alzheimer's disease pathogenesis by up-regulating BACE1 gene expression. *Proc. Natl. Acad. Sci. U.S.A.* **103**, 18727–18732 (2006). doi: 10.1073/pnas.0606298103; pmid: 17121991

14. X. Zhang et al., Hypoxia-inducible factor 1α (HIF-1α)-mediated hypoxia increases BACE1 expression and β-amyloid generation. *J. Biol. Chem.* **282**, 10873–10880 (2007). doi: 10.1074/jbc.M608856200; pmid: 17303576

15. K. Niwa et al., Aβ-peptides enhance vasoconstriction in cerebral circulation. *Am. J. Physiol. Heart Circ. Physiol.* **281**, H2417–H2424 (2001). doi: 10.1152/ajpheart.2001.281.6.H2417; pmid: 11709407

16. I. G. Gould, P. Tsai, D. Kleinfeld, A. Linninger, The capillary bed offers the largest hemodynamic resistance to the cortical blood supply. *J. Cereb. Blood Flow Metab.* **37**, 52–68 (2017). doi: 10.1177/0271678X16671146; pmid: 27780904

17. R. B. Nielsen et al., Capillary dysfunction is associated with symptom severity and neurodegeneration in Alzheimer's disease. *Alzheimers Dement.* **13**, 1143–1153 (2017). doi: 10.1016/j.jalz.2017.02.007; pmid: 28343848

18. C. M. Peppiatt, C. Howarth, P. Mobbs, D. Attwell, Bidirectional control of CNS capillary diameter by pericytes. *Nature* **443**, 700–704 (2006). doi: 10.1038/nature05193; pmid: 17036005

19. C. N. Hall et al., Capillary pericytes regulate cerebral blood flow in health and disease. *Nature* **508**, 55–60 (2014). doi: 10.1038/nature13165; pmid: 24670647

20. D. Attwell, A. Mishra, C. N. Hall, F. M. O'Farrell, T. Dalkara, What is a pericyte? *J. Cereb. Blood Flow Metab.* **36**, 451–455 (2016). doi: 10.1177/0271678X15610340; pmid: 26661200

21. E. Gutiérrez-Jiménez et al., Disturbances in the control of capillary flow in an aged APP^swe/PS1ΔE9 model of Alzheimer's disease. *Neurobiol. Aging* **62**, 82–94 (2018). doi: 10.1016/j.neurobiolaging.2017.10.006; pmid: 29131981

22. W. L. Klein, G. A. Krafft, C. E. Finch, Targeting small Aβ oligomers: The solution to an Alzheimer's disease conundrum? *Trends Neurosci.* **24**, 219–224 (2001). doi: 10.1016/S0166-2236(00)01749-5; pmid: 11250006

23. J. Attems, F. Lintner, K. A. Jellinger, Amyloid β peptide 1-42 highly correlates with capillary cerebral amyloid angiopathy and Alzheimer disease pathology. *Acta Neuropathol.* **107**, 283–291 (2004). doi: 10.1007/s00401-004-0822-6; pmid: 14986026

24. L. Alarcon-Martinez et al., Capillary pericytes express α-smooth muscle actin, which requires prevention of filamentous-actin depolymerization for detection. *eLife* **7**, e34861 (2018). doi: 10.7554/eLife.34861; pmid: 29561727

25. J. Palmer, S. Love, Endothelin receptor antagonists: Potential in Alzheimer's disease. *Pharmacol. Res.* **63**, 525–531 (2011). doi: 10.1016/j.phrs.2010.12.008; pmid: 21193044

26. C. Iadecola et al., SOD1 rescues cerebral endothelial dysfunction in mice overexpressing amyloid precursor protein. *Nat. Neurosci.* **2**, 157–161 (1999). doi: 10.1038/5715; pmid: 10195200

27. J. Kuroda et al., Nox4 is a major source of superoxide production in human brain pericytes. *J. Vasc. Res.* **51**, 429–438 (2014). doi: 10.1159/000369930; pmid: 25612841

28. Y. Zhang et al., An RNA-sequencing transcriptome and splicing database of glia, neurons, and vascular cells of the cerebral cortex. *J. Neurosci.* **34**, 11929–11947 (2014). doi: 10.1523/JNEUROSCI.1860-14.2014; pmid: 25186741

29. A. Zeisel et al., Molecular Architecture of the Mouse Nervous System. *Cell* **174**, 999–1014.e22 (2018). doi: 10.1016/j.cell.2018.06.021; pmid: 30096314

30. J. Luo, P. Grammas, Endothelin-1 is elevated in Alzheimer's disease brain microvessels and is neuroprotective. *J. Alzheimers Dis.* **21**, 887–896 (2010). doi: 10.3233/JAD-2010-091486; pmid: 20634595

31. J. C. Palmer, R. Barker, P. G. Kehoe, S. Love, Endothelin-1 is elevated in Alzheimer's disease and upregulated by amyloid-β. *J. Alzheimers Dis.* **29**, 853–861 (2012). doi: 10.3233/JAD-2012-111760; pmid: 22330820

32. D. Paris et al., Vasoactive effects of Aβ in isolated human cerebrovessels and in a transgenic mouse model of Alzheimer's disease: Role of inflammation. *Neurol. Res.* **25**, 642–651 (2003). doi: 10.1179/016164103101201940; pmid: 14503019

33. N. B. Hamilton, D. Attwell, C. N. Hall, Pericyte-mediated regulation of capillary diameter: A component of neurovascular coupling in health and disease. *Front. Neuroenergetics* **2**, 5 (2010). doi: 10.3389/fnene.2010.00005; pmid: 20725515

34. V. Della Bianca, S. Dusi, E. Bianchini, I. Dal Prà, F. Rossi, β-amyloid activates the O-2 forming NADPH oxidase in microglia, monocytes, and neutrophils. A possible inflammatory mechanism of neuronal damage in Alzheimer's disease. *J. Biol. Chem.* **274**, 15493–15499 (1999). doi: 10.1074/jbc.274.22.15493; pmid: 10336441

35. L. Park et al., Brain perivascular macrophages initiate the neurovascular dysfunction of Alzheimer Aβ peptides. *Circ. Res.* **121**, 258–269 (2017). doi: 10.1161/CIRCRESAHA.117.311054; pmid: 28515043

36. K. Špiranec et al., Endothelial C-type natriuretic peptide acts on pericytes to regulate microcirculatory flow and blood pressure. *Circulation* **138**, 494–508 (2018). doi: 10.1161/CIRCULATIONAHA.117.033383; pmid: 29626067

37. B. R. Roberts et al., Biochemically-defined pools of amyloid-β in sporadic Alzheimer's disease: Correlation with amyloid PET. *Brain* **140**, 1486–1498 (2017). doi: 10.1093/brain/awx057; pmid: 28383676

38. J. C. Cruz Hernández et al., Neutrophil adhesion in brain capillaries reduces cortical blood flow and impairs memory function in Alzheimer's disease mouse models. *Nat. Neurosci.* **22**, 413–420 (2019). doi: 10.1038/s41593-018-0329-4; pmid: 30742116

39. L. Park et al., Aβ-induced vascular oxidative stress and attenuation of functional hyperemia in mouse somatosensory cortex. *J. Cereb. Blood Flow Metab.* **24**, 334–342 (2004). doi: 10.1097/01.WCB.0000105800.49957.1E; pmid: 15091114

40. G. A. Carlson et al., Genetic modification of the phenotypes produced by amyloid precursor protein overexpression in transgenic mice. *Hum. Mol. Genet.* **6**, 1951–1959 (1997). doi: 10.1093/hmg/6.11.1951; pmid: 9302276

41. A. Mishra et al., Imaging pericytes and capillary diameter in brain slices and isolated retinae. *Nat. Protoc.* **9**, 323–336 (2014). doi: 10.1038/nprot.2014.019; pmid: 24434801

42. M. P. Lambert et al., Vaccination with soluble Aβ oligomers generates toxicity-neutralizing antibodies. *J. Neurochem.* **79**, 595–605 (2001). doi: 10.1046/j.1471-4159.2001.00592.x; pmid: 11701763

43. A. Jan, D. M. Hartley, H. A. Lashuel, Preparation and characterization of toxic Aβ aggregates for structural and functional studies in Alzheimer's disease research. *Nat. Protoc.* **5**, 1186–1209 (2010). doi: 10.1038/nprot.2010.72; pmid: 20539293

44. AmideBio, www.amidebio.com/wp-content/uploads/2016/07/Abeta_Quantitation_Protocol.pdf.

45. W. Huang et al., Novel NG2-CreERT2 knock-in mice demonstrate heterogeneous differentiation potential of NG2 glia during development. *Glia* **62**, 896–913 (2014). doi: 10.1002/glia.22648; pmid: 24578301

46. L.-J. Wu et al., The voltage-gated proton channel Hv1 enhances brain damage from ischemic stroke. *Nat. Neurosci.* **15**, 565–573 (2012). doi: 10.1038/nn.3059; pmid: 22388960

47. S. J. Won, J. E. Kim, G. F. Cittolin-Santos, R. A. Swanson, Assessment at the single-cell level identifies neuronal glutathione depletion as both a cause and effect of ischemia-reperfusion oxidative stress. *J. Neurosci.* **35**, 7143–7152 (2015). doi: 10.1523/JNEUROSCI.4826-14.2015; pmid: 25948264

48. M. P. Murphy, H. LeVine 3rd, Alzheimer's disease and the amyloid-β peptide. *J. Alzheimers Dis.* **19**, 311–323 (2010). doi: 10.3233/JAD-2010-1221; pmid: 20061647

49. T. Saito et al., Single App knock-in mouse models of Alzheimer's disease. *Nat. Neurosci.* **17**, 661–663 (2014). doi: 10.1038/nn.3697; pmid: 24728269

50. A. R. Pries, T. W. Secomb, P. Gaehtgens, J. F. Gross, Blood flow in microvascular networks. Experiments and simulation. *Circ. Res.* **67**, 826–834 (1990). doi: 10.1161/01.RES.67.4.826; pmid: 2208609

Science

Amyloid β oligomers constrict human capillaries in Alzheimer's disease via signaling to pericytes

Ross Nortley, Nils Korte, Pablo Izquierdo, Chanawee Hirunpattarasilp, Anusha Mishra, Zane Jaunmuktane, Vasiliki Kyrargyri, Thomas Pfeiffer, Lila Khennouf, Christian Madry, Hui Gong, Angela Richard-Loendt, Wenhui Huang, Takashi Saito, Takaomi C. Saido, Sebastian Brandner, Huma Sethi and David Attwell

Pericytes put the squeeze on cognition

Like a computer, the brain needs a reliable source of power, which is provided as oxygen and glucose in the blood. However, in many neurological disorders this energy supply is disrupted. Brain blood flow is controlled by adjustment of the diameters of the vessels supplying blood. Nortley *et al.* found that, both in humans developing Alzheimer's disease (AD) and in a mouse model of AD, brain capillaries become squeezed by pericytes (see the Perspective by Liesz). By defining the underlying mechanism, they suggest potential targets for therapy in early AD.

Science, this issue p. eaav9518; see also p. 223

ARTICLE TOOLS	http://science.sciencemag.org/content/365/6450/eaav9518
SUPPLEMENTARY MATERIALS	http://science.sciencemag.org/content/suppl/2019/06/19/science.aav9518.DC1
RELATED CONTENT	http://science.sciencemag.org/content/sci/365/6450/223.full http://stm.sciencemag.org/content/scitransmed/11/490/eaat8462.full http://stm.sciencemag.org/content/scitransmed/11/474/eaau6550.full http://stm.sciencemag.org/content/scitransmed/8/369/369ra178.full http://stm.sciencemag.org/content/scitransmed/8/363/363ra150.full
REFERENCES	This article cites 51 articles, 7 of which you can access for free http://science.sciencemag.org/content/365/6450/eaav9518#BIBL
PERMISSIONS	http://www.sciencemag.org/help/reprints-and-permissions

Use of this article is subject to the Terms of Service